Journal of materials and Environmental Sciences
ISSN : 2028-2508

JMES, 2017 Volume 8, Issue 1, Page 195-208

http://www.imaterenvironsci.com/

Quantum chemical calculations and corrosion inhibition efficiency of biopolymer "chitosan" on copper surface in 3%NaCl

R. Oukhrib, B. El Ibrahimi, H. Bourzi, K. El Mouaden, A. Jmiai, S. El Issami, L. Bammou, L. Bazzi*

Apply Chemistry-Physic Team, Materials and Environment Laboratory, IBN ZOHR Sciences Faculty, B.P.8106 Dakhla City, Agadir. Morocco.

Received 19 Oct 2016,
Revised 07 Nov 2016,
Accepted 10 Vov 2016

Keywords

- ✓ Corrosion inhibition,
- ✓ Copper, chitosan,
- ✓ NaCl 3%,
- ✓ Adsorption isotherm,
- ✓ Quantum chemical,
- ✓ Molecular dynamic

L Bazzi
l.bazzi@uiz.ac.ma
+212 0668062424

Abstract

The ability of chitosan biopolymer to inhibit the corrosion of copper in 3% NaCl solution was investigated experimentally and theoretically. In the first stage, the obtained results from electrochemical (polarization and impedance techniques) and weight loss measurements combined to morphology analysis reveal that this biopolymer act as a cathodic inhibitor and its inhibition efficiency (IE) increases with increasing of concentration to reach 86% at 1000 ppm. A slight decrease of IE was noted with increasing in temperature and the adsorption of chitosan on copper surface was found to obey Langmuir isotherm. In the second stage, the quantum chemical computations and molecular dynamics simulations showed that the studied compound was adsorbed differentially on the metal surface all depend to the nature of copper surface (Cu or Cu_2O) and the molecular structure of tested polymer.

1. Introduction

Owing to particular properties, the copper and its alloys are one of the most used materials today in high technological level and a wide range of industrial applications [1]. However, in some conditions these materials can undergo a corrosion phenomenon [2] .In this context, the protection of copper against corrosion in chloride containing aqueous media, like seawater, continues to attract attention [3–10].

For decades, the most used corrosion inhibitor for copper is Benzotriazole (BTA), owing to its high inhibitive ability and low cost [4,8]. Recently, due to imposed strict rules for the use and discharge of corrosion inhibitor by the environmental agencies [11], the use of BTA and its derivatives has been restricted worldwide due to their high toxicity [8]. This has resulted in high scientific interest and research activity in finding environment-friendly (called, green corrosion inhibitor) effective alternatives of BTA compounds [12–14]. Due to its molecular structure and non-toxicity, the biopolymer macro-molecule is one of potential candidate to safe protected metal against corrosion. The use of several carbohydrate polymers as metal corrosion inhibitors has been reviewed by S. A. Umoren et al. [15].

The chitosan is a linear polycation polysaccharide biopolymer (**Fig.1**) obtained by de-acetylation of chitin, the main component of crustacean carapace [16–20]. This natural polymer have properties such as biocompatibility and non-toxicity [21,22].

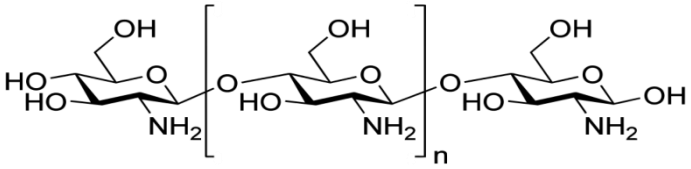

Figure 1: Molecular structure of chitosan biopolymer

In addition, chitosan is a soluble compound in aqueous media, without use of organic solvents[23]. Regarding these attracted properties, this paper aims to evaluate the ability of chitosan biopolymer to act as corrosion inhibitor for copper in 3% aqueous NaCl solution. Firstly, the issue is investigated experimentally using

potentiodynamic polarization, electrochemical impedance spectroscopy and weight loss methods combined to surface morphology analysis using scanning electron microscopy. Secondly, the quantum chemical calculations and molecular dynamic simulations approaches were employed to explain observed trends of tested biopolymer.

2. Technical detail

2.1. Experimental conditions

2.1.1. Materials and solution

Sodium chloride (Analytical Reagent®) and chitosan (Sigma-Aldrich®) showed in (**Fig. 1)** were used as received. A metallic copper rode (99.9%) were embedded in epoxy resin leaving a surface area of 1.0 cm^2 to contact tested solution for electrochemical experiments. Besides, the copper sheets used for weight loss measurements were mechanically cut into 1 cm × 1 cm × 0.1 cm dimensions.

The testing solution was prepared by 3.0 wt.% NaCl solution with different concentrations of chitosan (10, 50, 100 and 1000 ppm), and the solution without latest was treated as blank for comparison.

2.1.2. Electrochemical measurements

All electrochemical measurements were carried out in a conventional three-electrode cell with copper working electrode (WE), saturated calomel electrode (SCE) and wire platinum electrode was used. The temperature of solution was thermostatically controlled at 293 K using water thermostat IKA®-WERE system. Before each experiment, the WE was abraded with silicon carbide paper (grade 1200), degreased with acetone, and rinsed with distilled water before use. The measurement were performed with a PGZ301 (VoltaLab®) Potentiostat/Glvanostat. The WE was immersed in tested solution for 15 min at open circuit potential to reach a quasi-stationary potential. The electrochemical impedance spectroscopy (EIS) spectrum were recorded at this potential with a 10 mV as amplitude of the superimposed alternating current (AC) signal and the applied frequency ranged from 100 KHz to 10 Hz. The equivalent circuits of impedance data were analyzed by *ZsimpWin* software. The polarization curves were plotted from -600 to 200 mV/SCE at a polarization scan rate of 1 mV s^{-1}.

2.1.3. Weight loss measurements

Weight loss experiments were carried out in 100 mL glass beakers placed in a water thermostat (IKA®-WERE). Each copper specimen were mechanically ground by sandpaper (grade 1200) and degreased in acetone, then rinsed by distilled water, subsequently dried and weighed by analytical balance (SWISSQUALITY®). The copper samples in triplicate were immersed in 3% NaCl solution for each chitosan concentration at different temperatures (293, 303, 313 and 323 K), respectively. After 24 hours as immersion time, the specimens were rinsed thoroughly in 0.1 M HNO_3 solutions and by distillated water, subsequently dried and re-weighed. The corrosion rate (W) were calculated using the following equation (**Eq. 1**):

$$W = \frac{m_f - m_i}{A \, . \, t} \qquad \textbf{(Eq. 1)}$$

Where m_i and m_f are the weight (mg) before and after immersion in the tested solution, "A" the area of the specimens (cm^2), and "t" the exposure time (hour).

2.1.4. Surface morphology

The surface morphology of the copper specimens before and after immersed in 3% aqueous NaCl solution for 24 hours without and with 100ppm of chitosan at 298 K was observed by scanning electron microscope (FEI ESEM Quanta 200).

2.2. Computational details

2.2.1. Quantum chemical calculations

Quantum chemical computations were carried out by using *Gaussian 03* [24–26] software package, at density functional theory (DFT) with the Beck's three parameter exchange functional along with the Lee-Yang-Parr nonlocal correlation functional (B3LYP) with 6-31++G as basis set [27–33] in gas phase. However, regarding to the biggest of studied molecule (**Fig. 1**) and the limitations of used quantum chemical method (i.e. DFT/B3LYP 6-31++G), in this study the calculations were limited to two units (n = 0) from the chitosan polymer skeleton (**Fig. 2**).

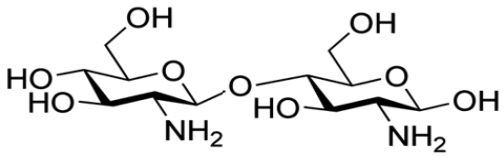

Figure 2: Used polymer fragment for the quantum chemical calculations

The following quantum descriptors were calculated from the obtained optimized structure: energy of highest occupied molecular orbital (E_{HOMO}), energy of lower unoccupied molecular orbital (E_{LUMO}), the gape energy between the last ($\Delta E_{LUMO-HOMO}$), dipole moment (μ), absolute electronegativity (χ, **Eq. 2**), global hardness (η, **Eq. 3**), and the number of transferred electrons (ΔN, **Eq. 4**). In order to calculate ΔN, we will adopt a value χ_{Cu}= 4.48 and η_{Cu} = 0 [34]. In addition, Mulliken partial charges and molecular orbitals distribution were calculated[35–38]:

$$\chi \approx -0.5\,(E_{HOMO} + E_{LUMO}) \quad \textbf{(Eq. 2)}$$

$$\eta \approx 0.5\,(E_{LUMO} - E_{HOMO}) \quad \textbf{(Eq. 3)}$$

$$\Delta N = \frac{\chi_{Cu} - \chi_{Inh}}{2\,(\eta_{Cu} + \eta_{Inh})} \quad \textbf{(Eq. 4)}$$

2.2.2. Molecular dynamics simulations

In aim to get more information about the interaction between investigated biopolymer and the substrate surface, molecular dynamics (MD) simulations were performed by using Adsorption Locator module implemented in the *Materials Studio 6.0* software [39,40]. For this propose, the effect of polymer chain length (**Fig. 1**) on the interaction of chitosan with substrate surface will be investigated. The latest was tested from two (n = 0) to ten unites (n = 8) in polymer fragment, with one unite as incremental steps. To design a possible lower energy adsorption configuration of those polymer fragments, the Metropolis Monte Carlo simulation is performed as the temperature of system is decreased [40].

The substrate was modeled by eight stoichiometric Cu_2O layers (thickness = 19.72 Å) without a metal support underneath, this due to two reasons. Firstly, in the context of corrosion under near-neutral pH conditions as our (i.e. 3 wt% NaCl), the oxidized surfaces of copper would be much more relevant to consider it [41]. Secondly, M. Finšgar et al. [42] reported that the average thickness of formed oxide on copper surface immersed in 3 wt% NaCl solution were estimated to be 22 ± 3 Å. In other hand, a great vacuum region with 60 Å thickness was built above Cu_2O (111) plan. The simulation was carried out with a single chitosan fragment polymer on the Cu_2O (111) crystal surface in a simulation box (66.4 Å × 66.4 Å × 79.7 Å) with periodic boundary conditions. Furthermore, to reveal the effect of chemical nature of surface on the interaction of designed polymers fragments, also, the Cu (111) surface will be studied [43]. The COMPASS (Condensed Phase Optimized Molecular Potentials for Atomistic Simulation Studies) force field was employed to optimize the structure of all components of the system. The electrostatic potential energy was calculated by the Ewald summation technique and the van der Waals potential energy was calculated by the atom based technique.

3. Results and discussion

3.1. Electrochemical polarization studies

The influence of various concentrations of chitosan compound on cathodic and anodic polarization curves of copper in 3 wt% NaCl medium at room temperature was shown in (**Fig. 3)**. By manual extrapolation of the Tafel line to the corrosion potential some polarization parameters were terminated. **Table 1** shows the corrosion potential (E_{corr}), corrosion current density (i_{corr}), anodic Tafel slope (β_a), and the efficiency of inhibition (IE_i) which calculated by following relation (**Eq. 5**):

$$IE_i(\%) = \left(1 - \frac{i'_{corr}}{i_{corr}}\right) \times 100 \quad \textbf{(Eq. 5)}$$

where i_{corr} and i'_{corr} are the corrosion current densities for in the presence and absence of chitosan, respectively.

On polarization curve for uninhibited system (**Fig. 3**), the anodic process of corrosion is associated to the transfer of metal ions from the metal surface into the solution, and the cathodic process is associated to the reduction of dissolved oxygen [44]. However, the addition of chitosan to saline solution was affected the anodic branch of the copper polarization curves, which reflected on anodic Tafel slop values (**Table 1**). This suggested that tested biopolymer modified the mechanism of copper corrosion in 3 wt% NaCl solution[10].

Furthermore, it is obvious that the presence of chitosan leads to decrease the current density when the concentration was increased, notably for cathodic current, and shifted of corrosion potential to the negative values. These results indicated that investigated biopolymer act as cathodic inhibitor. Inspection of the inhibition efficiency values given in **Table 1**, reveal that the inhibition efficiency increase by increasing inhibitor concentration to reach 79% at 1000ppm. So, these experiments showed the great ability of chitosan to act as a good corrosion inhibitor for copper in 3 wt% NaCl solution.

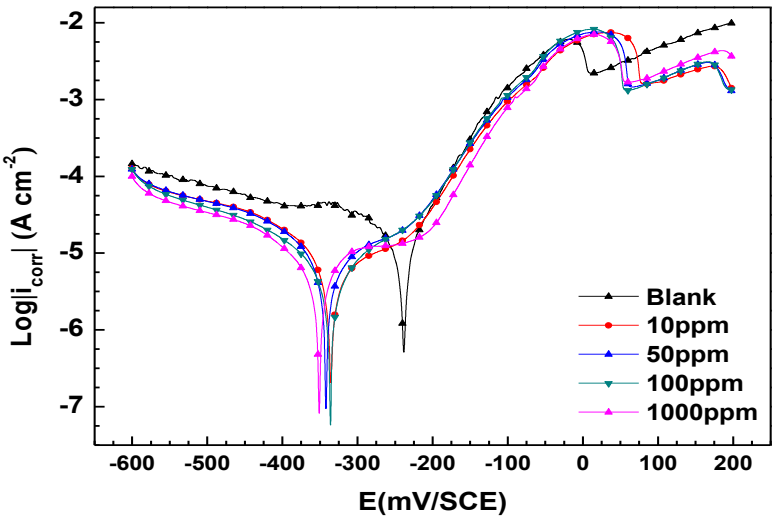

Figure 3: Potentiodynamic polarization curves of copper in 3 wt% NaCl solution without and with chitosan at different concentrations (at 293 K)

Table 1: Polarization parameters and efficiency of corrosion inhibition (IE_i) on copper by chitosan in 3 wt% NaCl solution (at 293 K)

Medium	E_{corr} (mV)	i_{corr} (μA cm^{-2})	β_a (mV dec^{-1})	IE_i (%)
Blank	-239	34.6	69	-
10 ppm	-334	20.0	81	42
50 ppm	-342	12.3	78	64
100 ppm	-334	08.7	74	75
1000 ppm	-349	07.2	72	79

3.2. Electrochemical impedance spectroscopy measurements

In order to get more information about corrosion mechanism and to confirm obtained results of polarization experiments, the AC-impedance measurements were carried out. The impedance spectra (in Nyquist format) of copper in 3 wt% NaCl solution without and with different concentrations of chitosan biopolymer are represented in (**Fig. 4)**.

As seen from (**Fig. 4)**, the spectrum impedance obtained in blank solution exhibit a deformed semicircle in the high frequency (HF) region followed by a straight line at low frequency (LF) range. Commonly, the HF semicircle could be assigned to the charge transfer and double layer characters. Whereas, the LF line is deemed as Warburg impedance (W), which can be interpreted by the diffusion of corrosive reactants to copper surface (as dissolved oxygen) or the transportation of corrosion product species (as soluble cuprous chloride complexes) to solution [6,37]. However, in the presence of chitosan, the diffusion Warburg line was disappeared. Along pressed semicircle are observed in the Nyquist plots (**Fig. 4**), demonstrating that copper corrosion is controlled by the charge transfer process in these conditions [45]. The same behaviours has noted by Y. Qiang *et al.* using 5-aminoindazole[5]**.** Moreover, the diameter of the semicircle for each tested concentrations of chitosan increases with its increasing, which indicate that better protection ability could be obtained at higher concentration of the biopolymer.

Used equivalent circuit models to fit experimental impedance data are depicted in (**Fig. 5)**. These circuits are composed from various electrical elements, namely: electrolyte resistance (R_S), resistance of protective film formed on copper surface (R_f), Warburg impedance (W), charge transfer resistance (R_{ct}) and the constant phase elements (CPE/n) [5].

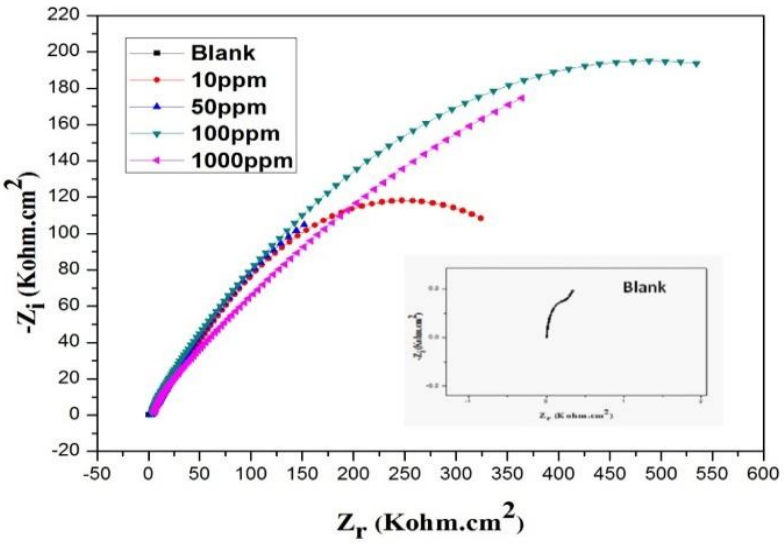

Figure 4: Nyquist plots of copper in 3 wt% NaCl solution containing different concentrations of chitosan.

As shown in (**Fig. 4)**, a good fit with used models circuits (**Fig. 5**) was obtained with our experimental data (the cross represent the fitted value). The obtained electrochemical parameters from fitting process are summarized in **Table 2**. The values of the inhibition efficiency (IE_R) of chitosan for copper in 3wt% NaCl solution are calculated as follows (**Eq. 6**):

$$IE_R(\%) = \left(1 - \frac{R_t}{R_{t(inh)}}\right) \times 100 \qquad \textbf{(Eq. 6)}$$

Where, R_t and $R_{t(inh)}$ are total resistance (polarization resistance) values in the absence and presence of the inhibitor, respectively. The total resistance is the sum of charge transfer resistance (R_{ct}) and film resistance (R_f). As can be seen from **Table 2**, the values of resistance (R_t) increase by increasing tested biopolymer concentration, in contrast, the CPE values tend to decrease. This suggesting that an efficiency protective film are formed by the adsorption phenomena of this macromolecule on copper surface [10]. The table results show that the inhibition efficiency of tested biopolymer increases with increasing of concentrations, and reach 83% at 1000ppm. Consequently, this compound acts as effective corrosion inhibitor for copper in 3 wt% aqueous NaCl solution.

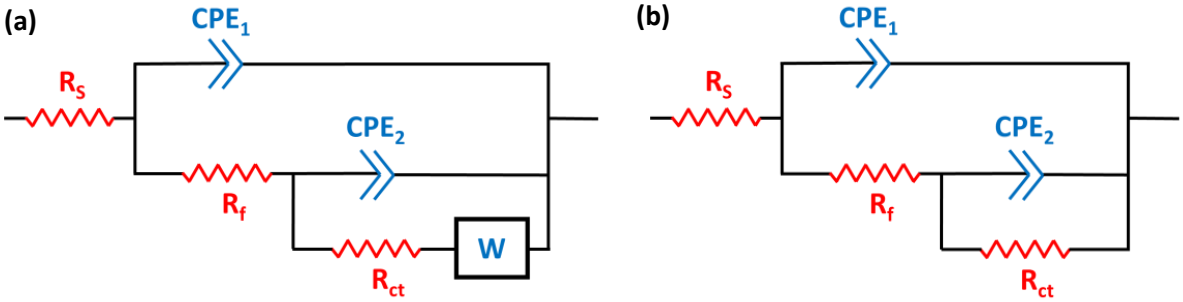

Figure 5: Equivalent circuits models used in the fitting of the impedance data of copper (a) without and (b) with chitosan in 3 wt% NaCl solution.

Table 2: Electrochemical impedance measurements of the copper in 3 wt% NaCl solution with and without different concentrations of chitosan biopolymer

Medium	R_S ($\Omega.cm^2$)	$R_t = R_f + R_{ct}$ ($\Omega.cm^2$)	CPE_1/n_1 ($S.s^n.cm^{-2}$)	CPE_2/n_2 ($S.s^n.cm^{-2}$)	W ($S.s^5.cm^{-2}$)	IE_R (%)
Blank	11.8	232.8	0.00719/0.946	0.00284/0.577	0.5396	-
10 ppm	3.2	480.5	0.00054/0.756	0.00284/0.577	-	52
50 ppm	2.2	635.6	0.00032/0.807	0.00506/0.520	-	63
100 ppm	2.0	980.4	0.00018/0.480	1.45E-5/0.997	-	76
1000 ppm	5.6	1350.5	3.65E-5/0.853	0.00218/0.397	-	83

3.3. Weight loss measurements

By using the weight loss measurements, the inhibition effect of tested biopolymer at various concentrations on corrosion of copper was investigated at different temperature after 24 hours of immersion. The inhibition efficiency (IE_W) values at different concentrations of this compound are calculated as follow (**Eq. 7**):

$$IE_w(\%) = \left(1 - \frac{W'}{W_0}\right) \times 100 \qquad \textbf{(Eq. 7)}$$

Where W_0 and W' are the corrosion rate of copper samples without and with chitosan after immersion time of 24 hours, respectively. The corrosion rate and the inhibition efficiency at different chitosan concentrations at 293 K are summarized in **Table 3**. The evolution of "W" and "IE_W(%)" according to the concentration of chitosan is represented graphically in (**Fig. 6)**. According to this data, it is clear that the corrosion rates decrease with increasing chitosan concentration, meanwhile the inhibition efficiency increase evidently in this sense to reach 87% at 1000 ppm, indicating good inhibitive capacity of this biopolymer. In other hand, these results are in a good agreement with those obtained from the electrochemical measurements (**sections III.1 and III.2**).

Table 3: Corrosion rate (W) and inhibition efficiency (IE_W) of copper corrosion by chitosan in 3 wt% NaCl solution at 293 K

Medium	**W (mg $cm^{-2}h^{-1}$) 10^3**	**IE_W (%)**
Blank	0.625	–
10 ppm	0.375	40
50 ppm	0.292	53
100 ppm	0.167	73
1000 ppm	0.083	87

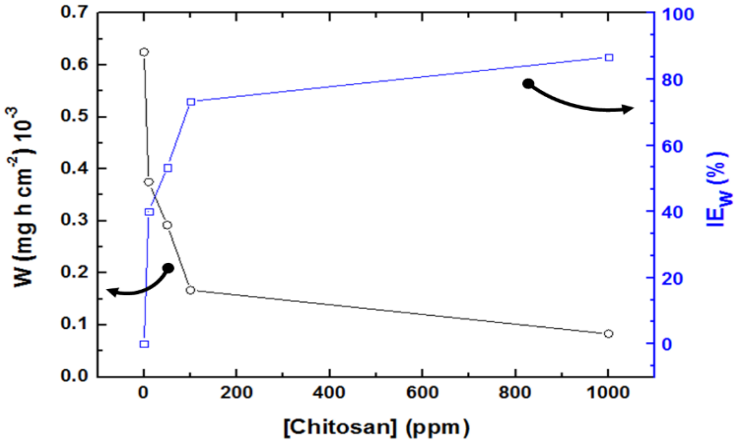

Figure 6: Corrosion rate of copper (O) and inhibition efficiency (□) of chitosan at different concentrations

3.3.1. Activation energy (E_a)

Through this study by using gravimetric method, we are taken gravimetric measurements at various temperatures (293, 303, 313 and 323 K) in the absence and presence of the inhibitor after 24 hours of immersion. The corresponding results are given in **Table 4**. As seen from **Table 4**, the corrosion rate, W, increases with the increasing temperature, both in free and inhibited solutions. Further, a slight change in values of inhibition efficiencies are observed in the range of temperature studied. Some information about adsorption mechanism of the inhibitor can be obtained from the activation energy values [46]. For this proposes, the Arrhenius equation was used (**Eq. 8**):

$$W = K \times \exp\left(-\frac{E_a}{RT}\right) \qquad \textbf{(Eq. 8)}$$

Where, k is the pre-exponential factor, $\mathbf{E_a}$ is the apparent activation energy of the corrosion process, R is the gas constant and T is the absolute temperature. **Figure 7** shows Arrhenius plots of the logarithm of the corrosion rate (W) vs 1000/T for copper in the corrosive medium with and without addition of chitosan at different concentrations. Straight-lines are obtained in free solution and in the presence of chitosan with correlation coefficients up to 0.850. The corresponding activation energies were calculated from the slopes of Arrhenius plots. The obtained values are given in **Table 4**. It is well known that similar or lower values of $\mathbf{E_a}$

in inhibited solutions compared to the free solution indicate the chemisorption mechanism, while higher values of $\mathbf{E_a}$ suggest the physical adsorption mechanism [47–49]. As seen in **table 4**, the calculated values of $\mathbf{E_a}$ increase compared to it in inhibitor free solution. This indicates a physisorption mechanism of the chitosan on copper surface leading to the formation of an adsorptive film of electrostatic character[50].

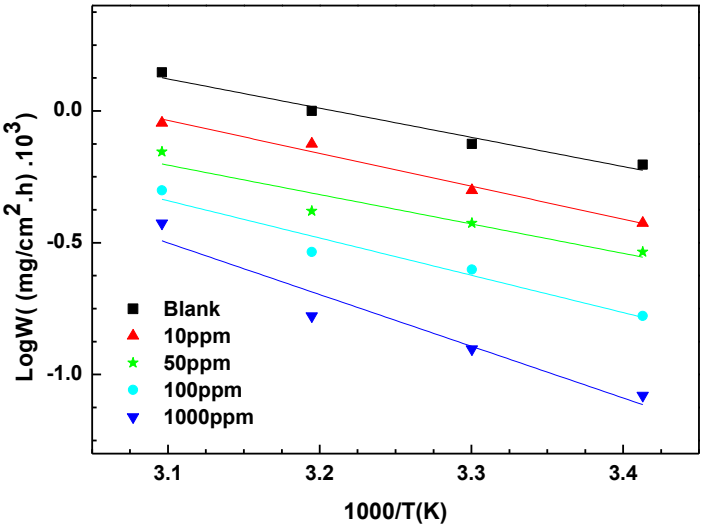

Figure 7: Log (W) vs. 1000/T for adsorption of chitosan.

Table 4: Corrosion rate (W) and activation parameter for copper in 3 wt% NaCl solutions in the absence and presence of chitosan at different concentrations

Medium	W (mg cm^{-2}h^{-1}) 10^3				IE_W (%)				E_a (KJ mol^{-1})
	293 K	303 K	313 K	323 K	293 K	303 K	313 K	323 K	
Blank	0.625	0.750	1.000	1.400	-	-	-	-	21.20
10 ppm	0.375	0.500	0.750	0.900	40	33	25	36	23.88
50 ppm	0.292	0.375	0.465	0.770	53	50	53	45	24.54
100 ppm	0.167	0.250	0.292	0.500	73	67	71	64	27.01
1000 ppm	0.083	0.125	0.167	0.375	87	83	83	73	37.93

3.3.2. Adsorption isotherm studies

Adsorption isotherm is widely used to get valuable information about the adsorption mechanism of corrosion inhibitor on metal/solution interface [51,52]. Chemical and physical adsorptions are two main kinds of adsorptions that explain the behaviors of inhibitors [53]. For this propose, several adsorption isotherms (Langmuir, Frumkin, Freundlich, etc.) are used to fit the results obtained from weight loss method of tested biopolymer. According to the linear determination coefficient (R^2) values, the Langmuir isotherm [54] (**Eq. 9**) was the best fit with our experiments data.

$$\frac{C}{\theta} = \frac{1}{K_{ads}} + C \qquad \textbf{(Eq. 9)}$$

where, the θ is the degree of surface coverage ($\theta = IE(\%) \times 0.01$), C is the concentration and K_{ads} (in dm^3 mol^{-1}) is the equilibrium constant of adsorption process. Thus, the adsorption process of chitosan on copper surface in 3 wt% NaCl solution obeys Langmuir isotherm. As can be seen in **Fig. 8**, the relationship between C/θ and C complies straight lines with intercept of $1/K_{ads}$. In other hand, the K_{ads} constant is related to the standard Gibbs free energy of adsorption ΔG°_{ads} (in Kj mol^{-1}) by the following equation [52] (**Eq. 10**):

$$K_{ads} = \frac{1}{55.5}\exp\left(-\frac{\Delta G^{\circ}_{ads}}{RT}\right) \qquad \textbf{(Eq. 10)}$$

Where, R (in J mol^{-1}K^{-1}) is the gaz constant, T (in K) is the absolute temperature, and 55.5 denotes the value of water molar concentration. The calculated thermodynamic parameters at different temperatures are listed in **Table 5**. As shown in table, the relatively high value of the adsorption equilibrium constant reflects the high adsorption ability of chitosan on the copper surface, which imply better inhibition efficiency. Generally, the

values of ΔG°_{ads} up to -20 kJ mol^{-1} are consistent with physisorption, while those around -40 kJ mol^{-1} or higher are associated with chemisorption as a result of the sharing or transfer of electrons from inhibitor molecules to the metal surface to form a coordinate bond [53]. In our study, the calculated ΔG°_{ads} values (**Table 5**) indicate that the adsorption of chitosan molecules is typically a physisorption mechanism, this result is confirmed by the determination of $\mathbf{E_a}$ value. In addition, the negative values of ΔG°_{ads} indicate that the adsorption of this inhibitor on copper surface is a spontaneous process [55].

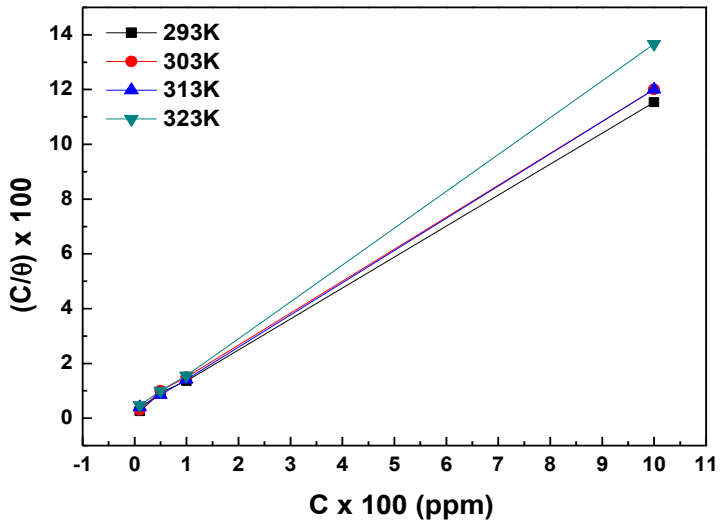

Figure 8: Plots of Langmuir adsorption isotherm (C/θ vs C) of chitosan on the copper surface at different temperatures

Table 5: Chitosan equilibrium constant and standard free energy of adsorption on copper in 3 wt% NaCl solution at different temperatures

Temperature (K)	**293**	**303**	**313**	**323**
K_{ads} (dm^3 mol^{-1})	1.12	1.17	1.17	1.34
ΔG^{o}_{ads} (kJ mol^{-1})	-10.07	-10.51	-10.86	-11.56

3.4 Morphological analysis

In order to get more information on the morphological features of metal surface and the effect of chitosan on this feature, the SEM analysis is widely used for this propose [56]. The high-definition photographs of the copper surface before and after 24 hours of immersion in 3 wt% NaCl solution with and without 100 ppm of chitosan were shown in (**Fig. 9)**. The surface morphology in blank solution (**Fig. 9 (b)**) was strongly corroded by the aggressive solution, and the surface of this specimen becomes rough, scratched and porous obviously when compared to the test specimens (**Fig. 9 (a)**). However, in the presence of chitosan (**Fig. 9 (c)**), the surface of the specimens is well protected and the micrographs are nearly the same as the freshly polished copper, indicating that the rate of corrosion was decreased. These observations confirm that tested biopolymer possesses a good inhibiting ability for copper corrosion in saline medium.

3.5. Quantum chemical calculations

As pointed out in earlier studies, the effectiveness of an inhibitor is related to the metal-inhibitor interactions which depends to the nature and the state of the metal surface and the chemical structure of the inhibitor [57–59]. In this study, quantum chemical calculations were conducted to investigate the relationship between molecular structure of the chitosan and its inhibition property. For this propose, two unites from the chitosan polymer were chosen to lead this calculation (**Fig. 1**). The geometry of the latest was fully optimized via DFT/B3LYP method employing 6-31G++ as basis set**.** The optimized molecular structure of selected unites, as well as, the HOMO and LUMO distributions are presented in **Fig. 10**.

In addition, the calculated quantum chemical parameters are listed in **Table 6**. As can be seen from **Fig. 10**, the HOMO orbital is located on the region around nitrogen ($-NH_2$) and oxygen atoms, which indicated theirs ability to be preferred active sites for an electronic donating process. Therefore, the favorite sites for interaction with the metal surface are located in these regions [60,61]. Further, the value of electron-donating

ability parameter (ΔN, **Table 6**) point out a possible electron transferring from atom on the metal surface to inhibitor molecule [59]. In this context, the ΔN has been often associated with inhibitor effectiveness [62].

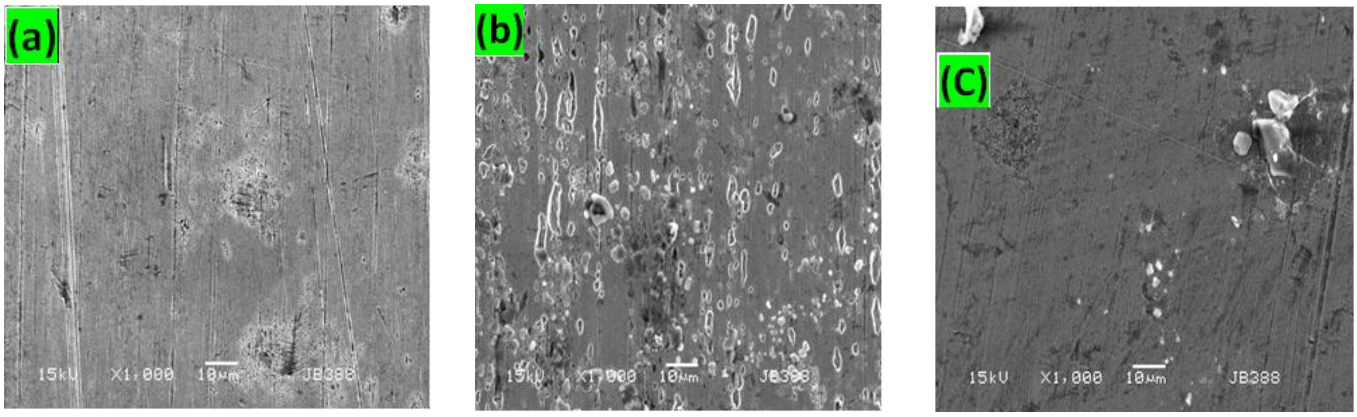

Figure 9: SEM images of (a) polished copper specimen and the specimens immersed in 3 wt% NaCl solution (b) without and with 100 ppm of chitosan (c) for 24 hours at 293 K.

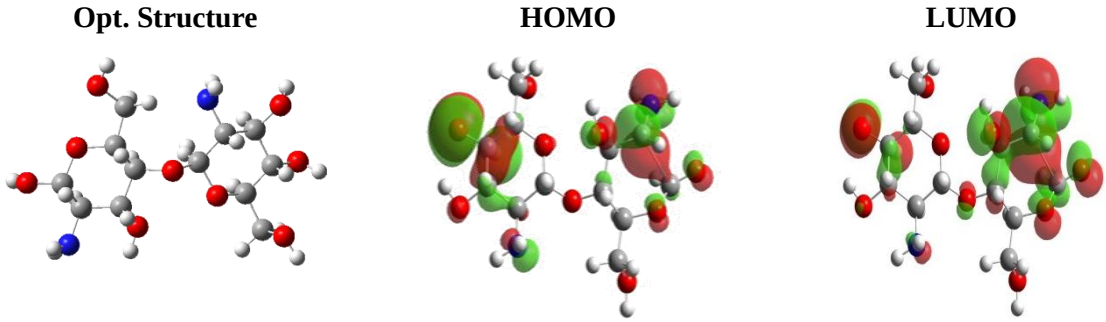

Figure 10: Optimized molecular structure and frontier molecular orbital (HOMO and LUMO) distribution of studied compound obtained by using DFT/B3LYP 6-31G++ method.

Table 6: Calculated quantum chemical parameters at DFT/B3LYP 6-31G++ level of theory in gas phase.

E_{HOMO} (eV)	E_{LUMO} (eV)	$\Delta E_{LUMO-HOMO}$ (eV)	χ (eV)	η (eV)	ΔN	μ (D)
-9.947	-6.618	3.329	8.282	1.665	-1.142	2.1979

There is a general consensus between several authors[62–67] that the presence of highest negative charge in some atoms give them more tendency to donate electrons to metal atoms than atoms with less negative charge. For this propose, one of the most common method to present this property is Mulliken analysis[62]. The Mulliken partial charges on carbon, oxygen and nitrogen atoms of studied compound are shown in (**Fig. 11)**.

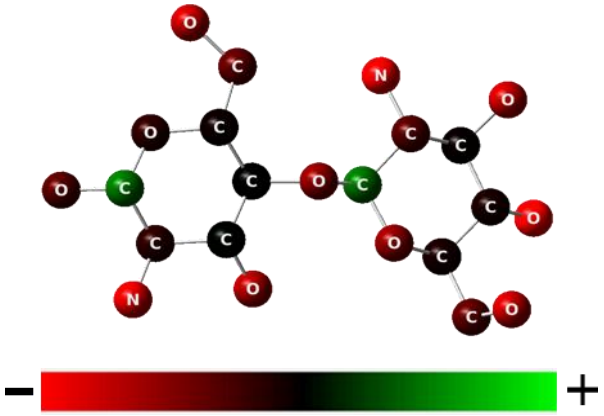

Figure 11: Mulliken charges distribution on the optimized structure of studied compound (without hydrogen atoms) using DFT/B3LYP 6-31G++ method in gas phase

It is clear that the highest negative charges are ported, especially, on the heteroatoms of –OH and $–NH_2$ groups. This distribution can make such groups as susceptible actives center to interact with cation metal on

the surface[59]. Furthermore, all negatives atoms on the molecular skeleton can contribute on this process through an intramolecular synergistic effect. Consequently, all those observations can explain the inhibition ability of chitosan against copper corrosion.

3.6. Molecular dynamics simulations

In order to get further information and to model the adsorption of inhibitor onto copper substrate, the molecular dynamics simulation has been performed in the present work. For this propose a comparative study on the adsorption of various biopolymer fragments (with, $0 \leq n \leq 8$) onto copper and its oxide (111) surfaces were carried out. Before putting them on the surface, all molecules were optimized first. As can be seen in (**Fig. 12)**, the energy[1] of biopolymer fragment increases linearly with the number of constituted unites (i.e. "*n*") of fragment.

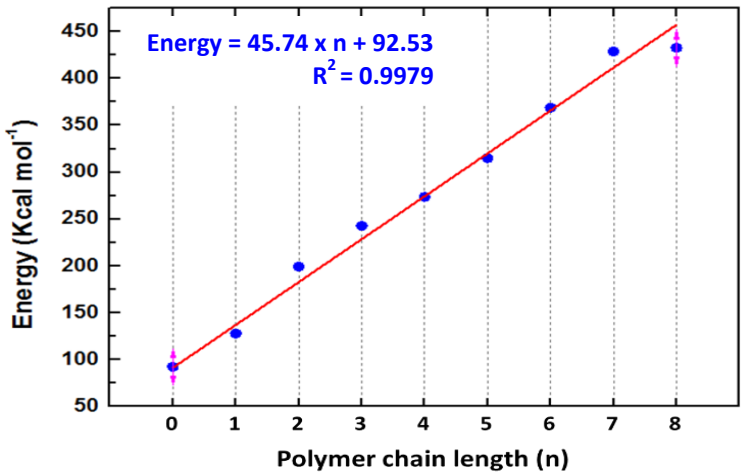

Figure 12: Energy of optimized molecules as a function of the polymer chain length (n)

An adsorption calculation was done on biopolymer fragment/copper substrate (without aqueous phase) to find the lowest energy for the whole system. The calculated adsorption energies (E_{ads}) are presented in (**Fig. 13)** both for Cu (111) and Cu_2O (111) as a function of monomer number.

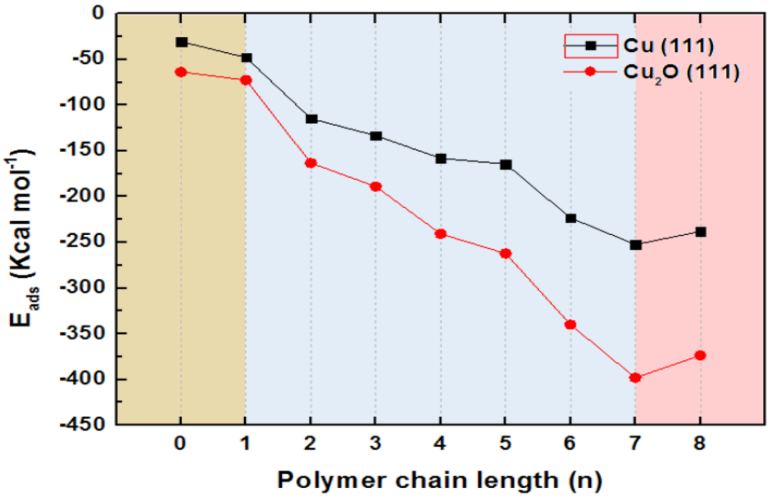

Figure 13: Calculated adsorption energy (E_{ads}) in function of polymer chain length (n)

As can be seen from this figure, the absolute adsorption energy increase as the number of monomer from n = 0 to 7 (brown and bleu area in **Fig. 13**) due to increasing in the adsorption sites number (i.e. O and N atoms). However, for 10 monomers (n = 8) the latest absolute energy was decreased (red area in **Fig. 13**). This behavior can be explained by the effect of sterically hindered, which reduce the stability of adsorbed molecule. The same trend was noted both for copper and oxide surfaces. In other hand, the chemical nature of metal surface has notably affected the values of calculated energy (i.e. E_{ads}). The Cu_2O (111) surface was exhibited the highest $|E_{ads}|$ values against theirs corresponding for Cu (111) surface (**Fig. 13**). This difference can be attributed to the presence of oxygen atoms on the surface, which improves the interaction with polymer atoms, especially the atoms with lower electronic density, such hydrogen which lead to formation the hydrogen bonds

[1] Those energies were calculated by using COMPASS force field.

[41]. Beside, more the polymer chain length increases, the difference increase in same sense. Those observations showed the importance to choose the appropriate substrate surface to model such interactions.

As discussed previously (**section II.2.2**), the appropriate surface to model the interaction of tested inhibitor and metallic substrate was copper oxide surface. For this reason, we limited to illustrate the shape of biopolymer fragments molecules on a stoichiometric Cu_2O (111) surface (see **Fig. 14**).

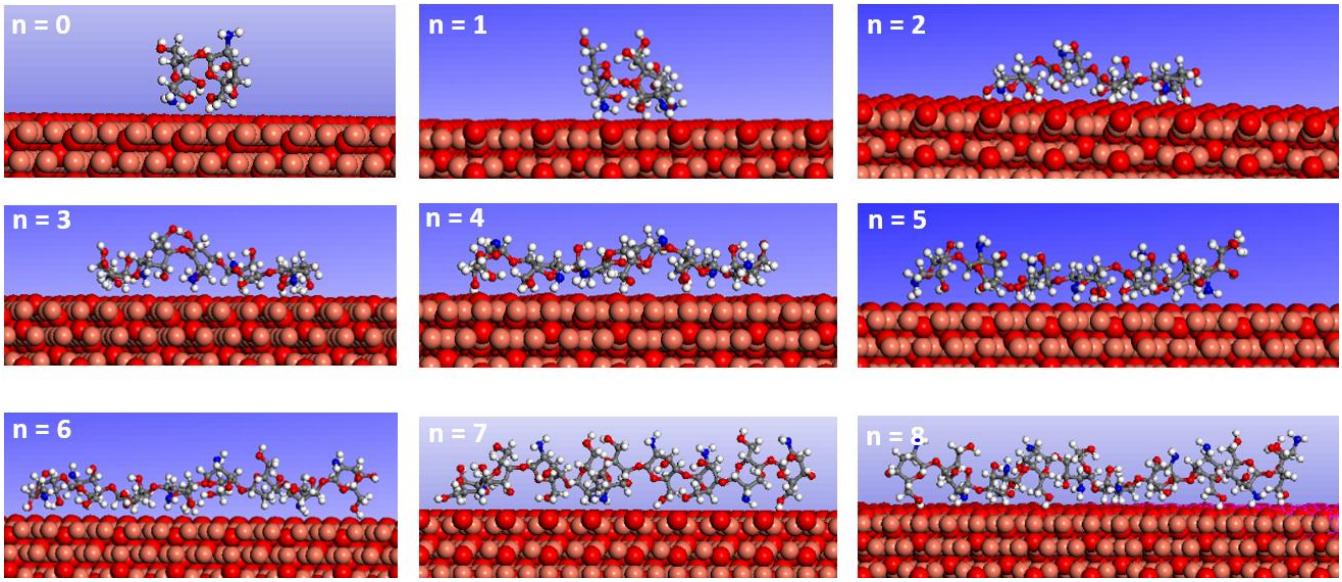

Figure 14: Equilibrium configuration for adsorption of different polymer fragments on Cu_2O (111) surface after optimization.

As shown in (**Fig. 14)** these molecules are interacted to surface through theirs heteroatoms and via hydrogen atoms by formation the hydrogen-bonds type: polymer–H···O–Metal. In addition, it can be observed that the equilibrium configuration of adsorbed molecules on target surface was depended to the "n" value. As noted, the fragments polymer molecules with $n \leq 1$ were interacted mainly by the extreme functional groups in theirs chain skeleton. However, for $n \geq 2$ the molecules were interacted through more function groups which imply a strong contact to oxide surface. This observation can explain the notable difference in their corresponding adsorption energy (**Fig. 13**). In basis to those results (**Fig. 15)** presents the simplified schemas of adsorbed polymer molecules with different length onto copper surface.

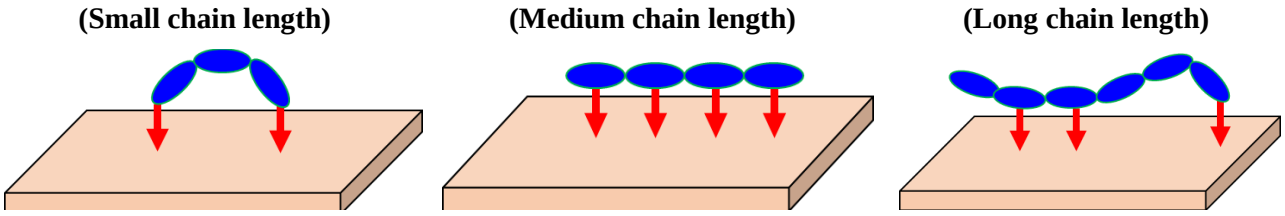

Figure 15: Simplified schema of adsorption mode for chitosan at different length chain onto copper surface

Conclusions

The effect of chitosan biopolymer on the corrosion inhibition of copper in 3 wt.% NaCl solution was studied experimentally and theoretically. The obtained results showed the ability of chitosan to acts as an effective eco-friendly corrosion inhibitor in studied conditions. Its inhibition efficiency increases by increasing inhibitor concentration to reach 86% at 1000 ppm. However, this ability has been slightly decreased with increasing of temperature. Further, the SEM micrographs confirmed the protection effect of chitosan. Electrochemically, the tested compound was found to affect the mechanism of copper dissolution. In whole, the electrochemical methods and weight loss measurements were in good agreement. In other hand, the inhibitory ability of chitosan was attributed to its electrostatic interaction with copper surface. The chemical computations results proved that the chitosan has showed a high ability to adsorb onto stoichiometric Cu_2O (111) regarding Cu (111) surface. Further to the interaction between the heteroatoms of polymer and copper cation on surface, this behavior has explained by the possibility to form hydrogen bonds in case of oxide surface. Concerning the molecular structure of tested biopolymer, it was found that the polymer chain length (noted "n") has a notable effect on the adsorption energy (E_{ads}). In this work, we limited to investigate the molecular adsorption at a

solid/vacuum interface. However, the aqueous phase would be much more relevant to consider in the context of corrosion. Therefore, in future publication this consideration will be taken in account.

Acknowledges-One of the authors (B. El Ibrahimi) expresses his appreciation for support from Morocco CNRST (Centre National pour la Recherche Scientifique & Technique) through the excellence scholarship of searching program (N°005UIZ2014, 2014 Edition).

References:

1. Ross R.B., *Metallic Materials Specifications Handbook*, (1992) 94.
2. La QueL., *Marine Corrosion Causes and Prevention*, (1975) 233.
3. Nam N.D., Thang V.Q., Hoai N.T., Van Hien P., Yttrium 3-(4-nitrophenyl)-2-propenoate used as inhibitor against copper alloy corrosion in 0.1M NaCl solution, E*val. Program Plann*. (2016) 1–11.
4. Kokalj A., The roles of mercapto, benzene and methyl groups in the corrosion inhibition of imidazoles on copper: I. Experimental characterization, *Corros. Sci*.98 (2015) 107–118.
5. Qiang Y., Zhang S., Xu S., Li W., Journal of Colloid and Interface Science Experimental and theoretical studies on the corrosion inhibition of copper by two indazole derivatives in 3 . 0 % NaCl solution, *J. Colloid Interface Sci.* 472 (2016) 52–59.
6. Chuan LiC., Yu Guo X., Shen S., Song P., Xu T., Wen Y., et al., Adsorption and corrosion inhibition of phytic acid calcium on the copper surface in 3wt% NaCl solution, *Corros. Sci*.83(2014) 147–154.
7. Milic M., Petrovic M.B., Antonijevic M.M., Films formed on copper surface in chloride media in the presence of azoles, *Corros. Sci.* 51 (2009) 1228–1237.
8. Hammouti B., Dafali A.,Touzani R., Bouachrine M., Inhibition of copper corrosion by bipyrazole compound in aerated 3 % NaCl, *J. Saudi Chem. Soc.* 16 (2012) 413–418.
9. Kear G., Barker B.D., WalshF.C., Electrochemical corrosion of unalloyed copper in chloride media—a critical review, *Corros. Sci*. 46 (2004) 109–135.
10. Hong S., Chen W., Zhang Y., Luo H.Q., Li M., Li N.B., Investigation of the inhibition effect of trithiocyanuric acid on corrosion of copper in 3 . 0 wt .% NaCl, *Corros. Sci*. 66 (2013) 308–314.
11. Vedula Sastri V. S., Green Corrosion Inhibitors: Theory and Practice, *John Wiley & Sons,Inc. Publication*(2011).
12. Raja M.G.S. P.B., Natural products as corrosion inhibitor for metals in corrosive media - A review, *Materials Letters*, 62 (2008) 113–116.
13. Gece G., Drugs: A review of promising novel corrosion inhibitors, *Corros. Sci.*, 53 (2011) 3873–3898.
14. Rani B.E.A., BasuB.B.J., Green Inhibitors for Corrosion Protection of Metals and Alloys : An Overview, *Int. J. Corros.*2012 (2012)15.
15. Umoren S.A., EduokU.M., Application of carbohydrate polymers as corrosion inhibitors for metal substrates in different media: A review, *Carbohydr. Polym*,140(2016) 314–341.
16. Crini G., BadotP., GuibalÉ., Chitine et chitosane du biopolymèr à l'application, *Press. Univ. Fr, Besançon*, (2009)19-54.
17. Justine D., PhD Thesis. Ecole Polytechnique - University of Nantes, 17 October 2006.
18. Montilla A., Ruiz-MatuteA.I., CorzoN., GiacominiC., IrazoquiG., Enzymatic generation of chitooligosaccharides from chitosan using soluble and immobilized glycosyltransferase (Branchzyme), *J. Agric. Food Chem.* 61 (2013) 10360–10367.
19. Rui-rong W., Guo J., Zhi-heng F., Broadband time-resolved elliptical crystal spectrometer for X-ray spectroscopic measurements in laser-produced plasmas, *Chin. Phys. B.*23 (2014) 21–25.
20. Sharp R., A Review of the Applications of Chitin and Its Derivatives in Agriculture to Modify Plant-Microbial Interactions and Improve Crop Yields, *Agronomy.* 3 (2013) 757–793.
21. T.H.E.E. Parliament, T.H.E. Council, O.F. The, E. Union, DIRECTIVE 2008/112/EC of the european parliament and of the council of 16 December 2008, Off. *J. Eur. Union.* (2008) 68–74.
22. Stęplewski W., Wawro D., Niekraszewicz A., Research into the Process of Manufacturing Alginate-Chitosan Fibres, *Fibres & Textiles in Eastern Europe*, 58 (2006) 25–31.
23. Agnihotri S. A., Mallikarjuna N.N., Aminabhavi T.M., Recent advances on chitosan-based micro- and nanoparticles in drug delivery, *J. Control. Release.* 100 (2004) 5–28.
24. Rivail J., Ruiz-lopezM., Quantum Modeling of Complex Molecular Systems (Book),*Springer International Publishing Switzerland*. 21(2015) 1-524.
25. Leszczynski J., Applications of Topological Methods in Molecular Chemistry (Book),*Springer International Publishing Switzerland*.22 (2016) 1-582.
26. Maia J.D.C., Urquiza Carvalho G.A., MangueiraC.P., SantanaS.R., CabralL.A.F., RochaG.B., GPU

linear algebra libraries and GPGPU programming for accelerating MOPAC semiempirical quantum chemistry calculations, *J. Chem. Theory Comput.* 8 (2012) 3072–3081.
27. Peralta J.E., Scuseria G.E., Cheeseman J.R., Frisch M.J., Basis set dependence of NMR spin-spin couplings in density functional theory calculations: First row and hydrogen atoms, *Chem. Phys. Lett.* 375 (2003) 452–458.
28. Tamilarasan R., SreekanthA., Spectroscopic and DFT investigations on the corrosion inhibition behavior of tris(5-methyl-2-thioxo-1,3,4-thiadiazole)borate on high carbon steel and aluminium in HCl media, *RSC Adv.* 3 (2013) 23681.
29. Rayne S., Forest K., A comparison of density functional theory (DFT) methods for estimating the singlet-triplet (S0-T1) excitation energies of benzene and polyacenes, Comput. *Theor. Chem.* 976 (2011) 105–112.
30. Barone V., Provasi P.F., Peralta J.E., Snyder J.P., Sauer S.P.A, Contreras R.H., Substituent effects on scalar 2J(19F,19F) and 3J(19F,19F) NMR couplings: A comparison of SOPPA and DFT methods, *J. Phys. Chem. A.* 107 (2003) 4748–4754.
31. Scalmani G., Frisch M.J., Mennucci B., Tomasi J., Cammi R., Barone V., Geometries and properties of excited states in the gas phase and in solution: Theory and application of a time-dependent density functional theory polarizable continuum model, *J. Chem. Phys.* 124 (2006) 094107.
32. Peralta J.E., Scuseria G.E., Density Functional Theory Calculation of Indirect Nuclear Magnetic Resonance Spin - Spin Coupling Constants in C_{70}, *J. AM. CHEM. SOC.*126 (2004) 7428–7429.
33. Palvimo J.J., Ihalainen J.A., Design, Synthesis, and Biological Evaluation of Nonsteroidal Cycloalkane [d]isoxazole-Containing Androgen Receptor Modulators, *Med. Chem. (Los. Angeles).*55(2012)6316−6327.
34. Pearson R.G., Absolute Electronegativity and Hardness: Application to Inorganic Chemistry,*Inorg. Chem.*27 (1988) 7684–7690.
35. Chetouani A., Aouniti A., Hammouti B., Benchat N., Benhadda T., Kertit S., Corrosion inhibitors for iron in hydrochloride acid solution by newly synthesised pyridazine derivatives, *Corros. Sci.* 45 (2003) 1675–1684.
36. Dagdag O., El Harfi A., El Gouri M., Touhami M.E., Essamri A., Cherkaoui O., Electrochemical impedance spectroscopy (SIE) evaluation of the effect of immersion time of the protective matrix based on a polymer Tetra Glycidyl of Ethylene Dianiline (TGEDA) on carbon steel in 3 % NaCl, *Int. J. ChemTech Res.* 9 (2016) 390–399.
37. Kumar S.R., Panigrahi M.K., Thakur S.K., Kainer K.U., Chakraborty M., Dhindaw B.K., Characterization of stress in reinforcements in magnesium based squeeze infiltrated cast hybrid composites, *Mater. Sci. Eng.* 415 (2006) 207–212.
38. Solmaz R., Altunbaş E., Kardaş G., Adsorption and corrosion inhibition effect of 2-((5-mercapto-1,3,4-thiadiazol-2-ylimino)methyl)phenol Schiff base on mild steel, *Mater. Chem. Phys.* 125 (2011) 796–801.
39. Frenkel B., Smit D., Understanding molecular simulation: from algorithms to applications (Book), *Elsevier (Computational sciences series),* 1 (2002) 1 – 638.
40. Url S., Archive T.J., Archive T., Optimization by Simulated Annealing, *Sci. New Ser.* 220 (2007) 671–680.
41. Kokalj A., The roles of mercapto, benzene, and methyl groups in the corrosion inhibition of imidazoles on copper: II. inhibitor–copper bonding, *Corros. Sci.*98 (2015)107–118.
42. Finšgar M., Peljhan S., Kokalj A., Milošev I., Determination of the Cu_2O Thickness on BTAH-Inhibited Copper by Reconstruction of Auger Electron Spectra, *J. Electrochem. Soc.*157(2010) 295-301.
43. Haghighi S.M., PhD Thesis. Pierre and Marie Curie University of Paris, 1 February 2016.
44. DehdabM., YavariZ., DarijaniM., BargahiA., The inhibition of carbon-steel corrosion in seawater by streptomycin and tetracycline antibiotics : An experimental and theoretical study, *Desalination.*400 (2016) 7–17.
45. Wang D., Xiang B., Liang Y., Song S., Liu C., Corrosion control of copper in 3.5 wt.% NaCl Solution by Domperidone: Experimental and Theoretical Study, *Corros. Sci.* 85 (2014) 77–86.
46. Liu P., Fang X., Tang Y., Sun C., Yao C., Electrochemical and Quantum Chemical Studies of 5-Substituted Tetrazoles as Corrosion Inhibitors for Copper in Aerated 0 . 5 M H 2 SO 4 Solution, *Mater. Sci. Appl.* 2011 (2011) 1268–1278.
47. Behpour M., Ghoreishi S. M., Gandomi-Niasar A., Soltani N., Salavati-Niasari M., The inhibition of mild steel corrosion in hydrochloric acid media by two Schiff base compounds SH SH, *J Mater*

*Sci.*44(2009) 2444–2453.
48. Aloui S., Forsal I., Sfaira M., Touhami M.E., Taleb M., Baba M.F., et al., New Mechanism Synthesis of 1, 4-Benzothiazine and its Inhibition Performance on Mild Steel in Hydrochloric Acid, Port. *Electrochim. Acta.* 27 (2009) 599–613.
49. Zarrouk A., Warad I., Hammouti B., Dafali A., Benchat N., The Effect of Temperature on the Corrosion of Cu / HNO 3 in the Presence of Organic Inhibitor : Part-2, *Int. J. Electrochem. Sci.* 5 (2010) 1516–1526.
50. Bouklah M., Hammouti B., Lagrenée M., Bentiss F., Thermodynamic properties of 2,5-bis(4-methoxyphenyl)-1,3,4-oxadiazole as a corrosion inhibitor for mild steel in normal sulfuric acid medium, *Corros. Sci.* 48 (2006) 2831–2842.
51. Li X., Deng S., Fu H., Inhibition of the corrosion of steel in HCl, H 2SO 4 solutions by bamboo leaf extract, *Corros. Sci.* 62 (2012) 163–175.
52. Mihit M., El Issami S., Bouklah M., Bazzi L., Hammouti B., The inhibited effect of some tetrazolic compounds towards the corrosion of brass in nitric acid solution, *Appl. Surf. Sci.* 252 (2006) 2389–2395.
53. Branzoi V., Branzoi F., Baibarac M., The inhibition of the corrosion of Armco iron in HCl solutions in the presence of surfactants of the type of N -alkyl quaternary ammonium salts, *Mater. Chem. Phys.* 65 (2000) 288–297.
54. Mora N., Cano E., Polo J.L., Puente J.M., Bastidas J.M., Corrosion protection properties of cerium layers formed on tinplate, *Corros. Sci.* 46 (2004) 563–578.
55. Zhou Y., Zhang S., Guo L., Xu S., Lu H., Gao F., Studies on the Effect of a Newly Synthesized Schiff Base Compound on the Corrosion of Copper in 3 % NaCl Solution, *Int. J. Electrochem. Sci.* 10 (2015) 2072–2087.
56. Li W., He Q., Pei C., Hou B., Experimental and theoretical investigation of the adsorption behaviour of new triazole derivatives as inhibitors for mild steel corrosion in acid media, *Electrochim. Acta.* 52 (2007) 6386–6394.
57. Khaled K.F., Electrochemical investigation and modeling of corrosion inhibition of aluminum in molar nitric acid using some sulphur-containing amines, *Corros. Sci.* 52 (2010) 2905–2916.
58. Obot I.B., Obi-Egbedi N.O., Umoren S.A., Adsorption characteristics and corrosion inhibitive properties of clotrimazole for aluminium corrosion in hydrochloric acid, *Int. J. Electrochem. Sci.* 4 (2009) 863–877.
59. El Ibrahimi B., Soumoue A., Jmiai A., Bourzi H., Oukhrib R., Computational study of some triazole derivatives (un- and protonated forms) and their copper complexes in corrosion inhibition process, *J. Mol. Struct.* 125(2016) 93–102.
60. Ash S., De S.P., Pyne S., Misra A., Excited state intramolecular proton transfer in 3-hydroxy flavone and 5-hydroxy flavone: A DFT based comparative study, *J. Mol. Model.* 16 (2010) 831–839.
61. Obot I.B., Obi-EgbediN.O., UmorenS.A., The synergistic inhibitive effect and some quantum chemical parameters of 2,3-diaminonaphthalene and iodide ions on the hydrochloric acid corrosion of aluminium, *Corros. Sci.* 51 (2009) 276–282.
62. Gece G., The use of quantum chemical methods in corrosion inhibitor studies, *Corros. Sci.* 50 (2008) 2981–2992.
63. Şafak S., Duran B., Yurt A., Türkoğlu G., Schiff bases as corrosion inhibitor for aluminium in HCl solution, *Corros. Sci.* 54 (2012) 251–259.
64. Döner A., Solmaz R., Özcan M., Kardas G., Experimental and theoretical studies of thiazoles as corrosion inhibitors for mild steel in sulphuric acid solution,*Corros. Sci.* 53 (2011) 2902–2913.
65. Karada F., Investigation of adsorption characteristics of methionine at mild steel / sulfuric acid interface : An experimental and theoretical study, Colloids Surfaces A Physicochem. *Eng. Asp.* 316 (2008) 55–61.
66. Gokhan G., Semra B., A theoretical study on the inhibition efficiencies of some amino acids as corrosion inhibitors of nickel, *Corros. Sci.* 52 (2010) 3435–3443.
67. Zhang J., Qiao G., Hu S., Yan Y., Ren Z., Yu L., Theoretical evaluation of corrosion inhibition performance of imidazoline compounds with different hydrophilic groups, *Corros. Sci.* 53 (2011) 147–152.